

Crustal Structure of the Molucca Sea Collision Zone, Indonesia

ROBERT McCAFFREY AND ELI A. SILVER

Earth Sciences Board, University of California, Santa Cruz, California 95064

RUSSELL W. RAITT

Scripps Institution of Oceanography, A-005, La Jolla, California 92093

Seismic refraction profiles run within the Molucca Sea of eastern Indonesia reveal a thick, low-velocity layer (collision complex) which we infer to be the source of the large negative free air gravity values associated with this arc-arc collision zone. Thicknesses of low-density material of up to 15 km beneath 2 km of water can account for the free air gravity anomaly, which reaches values as low as -230 mGal. To the east of the north trending Talaud-Mayu Ridge, which bisects the Molucca Sea, refraction profiles give depths to basement of 11.4 km, 15 km, and 10.7 km below sea level. One profile run west of the Talaud-Mayu Ridge in the central Molucca Sea shows basement to be several kilometers shallower than is observed 50 km to the east. This difference in depths to basement on either side of the Molucca Sea may be due to major faulting beneath the Talaud-Mayu Ridge and accounts for the strongly asymmetric shape of the regional gravity field over this basin. Crustal offsets totaling 6 km and stepped down to the west away from the Halmahera arc are inferred from one refraction profile run west of southern Halmahera. Complex travel time curves and high seismic attenuation are characteristic of refraction profiles run within the Molucca Sea collision complex. The collision complex can be interpreted as being composed of two distinct constant velocity layers. The upper layer has a compressional velocity averaging 2.0 km/s and thickness ranging from 2.5 to 3.5 km. The lower layer is much more varied in velocity (2.4–4.1 km/s) and thickness (8–11 km). Interpretations of travel time curves assuming constant vertical velocity gradients within the collision complex give equally well fitted solutions with gradients ranging mainly between 0.10 and 0.25 km/s per kilometer depth. The overall similarity between travel time curves coupled with anomalous travel times on the scale of a few kilometers suggests the internal structure of the collision complex to be that of blocks with dimensions of the order of several tens of kilometers embedded in a deformed matrix showing a continuous and nearly linear increase in compressional velocity with depth. We infer from a Bouguer gravity peak, 40 km wide and 50 mGal above the regional field, over the Talaud-Mayu Ridge in the vicinity of Mayu Island and the exposures of peridotite and gabbro on Mayu that a slice (or slices) of oceanic crust and upper mantle has been thrust upward at a steep angle beneath the ridge.

Introduction

Stable convergent plate boundaries are characterized by subduction of oceanic lithosphere beneath less dense continental margins or island arcs [McKenzie, 1969]. Complications arise, however, when buoyant lithospheric elements such as island arcs, seamounts, and continents approach the trench-arc system from the seaward side either by overriding the intervening ocean basin or as passive riders on subducting plates. Collisions between these nonsubductable features produce widespread zones of deformation and subsequent shifting of convergence to a more stable configuration. Such collisions are felt to be of primary importance in the orogenic process [Dewey and Bird, 1970].

Located at the junction of the Pacific, Philippine Sea, Eurasian, and Australian plates, the Molucca Sea in eastern Indonesia is the site of the only known example of an active collision between facing island arcs (Figure 1). The east facing Sangihe volcanic arc on the west and the west facing Halmahera arc on the east act to enclose the structurally symmetric collision area (Figure 2). The two magmatic arcs, convex toward one another at a minimum separation of 250 km, are associated with intermediate and deep Benioff zones which dip away from the central Molucca Sea [Hatherton and Dickinson, 1969; Hamilton, 1974; Cardwell et al., this volume]. Trapped between the encroaching island arcs is a highly deformed unit of varying lithologies, previously termed a melange wedge [Hamilton, 1979] or collision complex [Silver and Moore, 1978]. This body forms a topographic high, the Talaud-Mayu Ridge, which bisects the Molucca Sea parallel to the island arcs. Dredge hauls and surface exposures on the islands of the Talaud-Mayu Ridge show that part of the collision complex may be a tectonic melange consisting of blocks of peridotite, gabbro, pillow basalt, metamorphic rocks, and sediments [Silver and Moore, 1978; Hamilton, 1979], seen on the island of Talaud (Figure 1) to be surrounded by a scaly clay matrix [Sukanto, 1979]. A zone of very high earthquake activity subparallel to the Talaud-Mayu Ridge between Halmahera and Sulawesi shows predominantly thrust type focal mechanism solutions with slip vectors invariably perpendicular to the trend of the island arcs [Fitch, 1970, 1972; Fitch and Molnar, 1970; Cardwell et al., this volume]. The onset of back arc thrusting west of the Sangihe arc as interpreted by Hamilton [1979] is evidence for a jump in the subduction zone—a polarity reversal—as this collision nears completion.

In attacking the problem of the structure and tectonics of the Molucca Sea collision zone we have used mainly three geophysical tools: seismic reflection, seismic refraction, and gravity profiling. Islands are small and few, but the limited surface geologic data constrain the collision process. Seismic reflection interpretations will not be described in detail here because more extensive treatments are given by Silver and Moore [1978] and Hamilton [1979]. Published profiles show the material trapped between the island arcs to be highly deformed, interpreted

by Silver and Moore [1978] as spreading gravitationally away from the central Talaud-Mayu Ridge while overriding the slopes of the confining island arc aprons. The undeformed island arc apron sediments appear to become incorporated into the collision complex along thrust surfaces verging opposite to the sense of subduction [Silver and Moore, 1978].

This paper presents the results of 11 marine seismic refraction profiles run within the Molucca Sea collision zone of eastern Indonesia. Also presented are two long gravity profiles crossing the Molucca Sea collision zone perpendicular to the island arcs and cross-sectional models which satisfy refraction, gravity, and geologic data.

Seismic refraction profiles reported in this paper show that the collision complex is indeed anomalously thick in the central regions of the Molucca Sea and thins toward the Sangihe and Halmahera island arcs. This great thickness of low-density material is inferred to be the cause of the observed large negative free air gravity anomalies over this shallow water basin. Furthermore, a local gravity high over the Talaud-Mayu Ridge cannot be explained by the attraction of a low-density ridge alone and requires a large mass of material more dense than the collision complex. The presence and disposition of peridotite and gabbro on the Talaud-Mayu Ridge suggests that this local mass excess may be due to a steeply inclined slice (or slices) of oceanic crust and upper mantle having been incorporated into the collision complex during some stage of the collision.

Refraction Interpretations

Eleven seismic refraction profiles were shot in the Molucca Sea during legs 8 and 10 of the INDOPAC expedition on board the R/V *Thomas Washington* of Scripps Institution of Oceanography during late 1976 and early 1977. All were single-ship profiles employing either moored sonobuoys in reversed profiles or multiple drifting sonobuoys in open-ended profiles. A tabulation of results is given in Table 1, and locations of profiles are shown in Figure 2.

Most of the refraction profiles run in the Molucca Sea reveal irregular structure and high attenuation within the collision complex. These observations serve to characterize the collision complex further as highly deformed material. Extensive deformation is probably widespread throughout this thick unit and in the underlying basement.

High attenuation in the collision complex allowed resolution of refracted arrivals only to shot-detector distances of 60 km at most using explosive charges of up to 20 kg. Even greater attenuation was observed in profiles run to the west of the Talaud-Mayu Ridge, where larger shot weights were consistently needed. The increase in attenuation toward the Sangihe arc may reflect a greater degree of deformation within the collision complex on that side. This is consistent with a faster rate or longer duration of subduction at the Sangihe arc as is inferred from the contrasting lengths of Benioff zones beneath the Sangihe arc

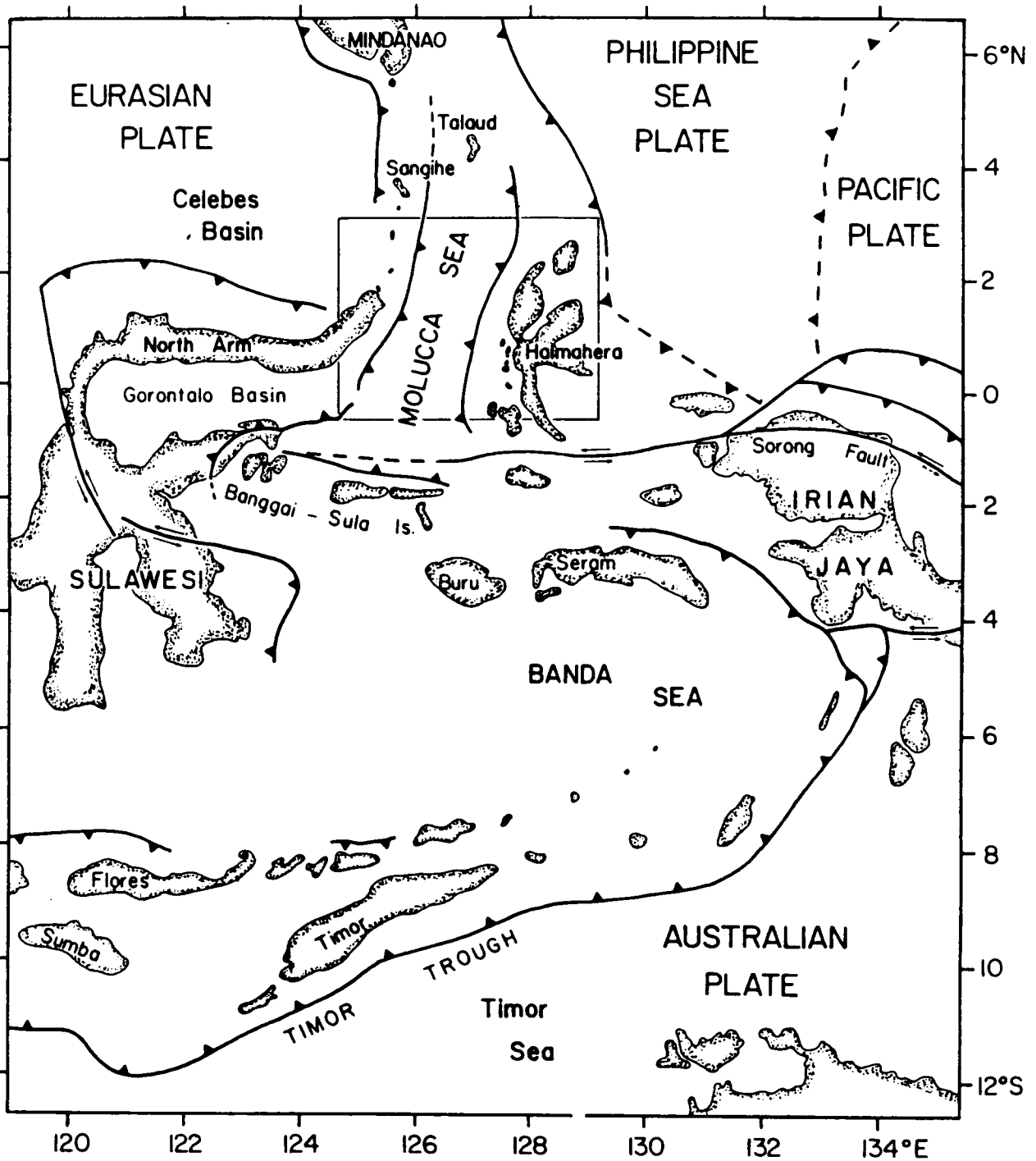


Fig. 1. Regional tectonic map of eastern Indonesia modified from Silver [1979] and Hamilton [1979]. Teeth along thrust faults are on overriding plate. The box surrounding the Molucca Sea shows area covered by Figure 2.

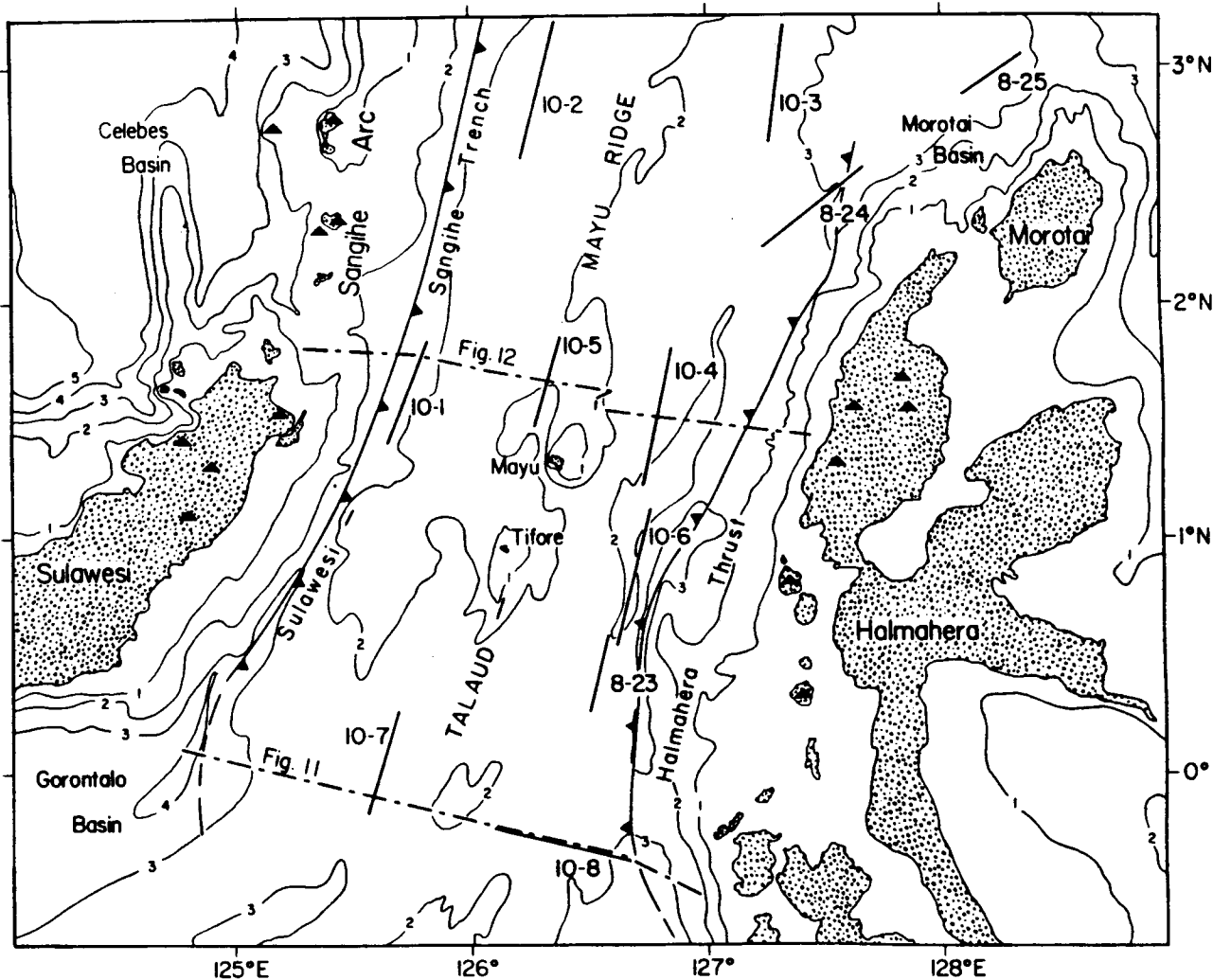


Fig. 2. Map of the Molucca Sea, eastern Indonesia, showing locations of seismic refraction lines (solid straight lines) and gravity traverses (dashed-dotted lines). Thrust faults are shown with teeth on hanging wall. Triangles represent active volcanoes defining the Sangihe and Halmahera magmatic arcs. Isobath interval is 1 km from *Mammerickx et al.* [1976].

(greater than 600 km) and the Halmahera arc (260 km) [*Hatherton and Dickinson, 1969*].

Plane layer solutions were found for those profiles whose plots of travel time versus distance exhibited a fair degree of linearity and whose reciprocal times, in reversed profiles, were in agreement. Lines 10-1, 10-2, 10-3, 10-6, and 8-25 fit these criteria. The remaining six profiles (10-4, 10-5N, 10-5S, 10-7, 10-8, 8-23, and 8-24) were analyzed by a graphical ray-tracing technique by which ray paths are drawn and interfaces modified until agreement, within estimated error, between the calculated and observed travel times is reached. This method was found to be much more effective when dealing with complex travel time curves

such as are observed in the Molucca Sea. A description of methods of analysis and errors involved is given in the appendix.

Five refraction profiles in the eastern part of the Molucca Sea give arrivals with apparent velocity of greater than 5.5 km/s (Table 1). This velocity serves as an indicator of basement in this area because it is well above the average velocity for upper oceanic crust [*Raitt, 1963; Christensen and Salisbury, 1975*]. Two reversed profiles (10-4 and 10-6) yield basement velocities of 6.5 and 7.1 km/s. Lines 10-5 and 10-8 were reversed, but coverage of the basement was obtained in only one direction.

Basement apparently shallows toward the Halmahera

TABLE 1. Molucca Sea Refraction Results

Profile	Type	Collision Complex							Figure	
		Average Water Depth, km	Upper Layer		Lower Layer		Basement			
			Velocity, km/s	Depth, km	Velocity, km/s	Depth, km	Velocity, km/s	Depth, km		
10-1	one-way multiple receiver	2.00	1.7	2.0				5.7	7-9	10
10-2	one-way multiple receiver	1.52	1.9	1.5-2.0	(2.43)	4.3				8
10-3	one-way multiple receiver	2.21	2.2	2.3-3.0	(4.3)	5.0				3
10-4	reversed	2.15	2.0	2.0-2.3	2.8	5.0	6.5		14-16	3
10-5S	one-way single receiver	1.57	2.2	1.6-2.0	(2.5)	4.0	7.0*		10-12	8
10-5N	one-way single receiver	1.52	1.9	1.5	3.8	2-4				9
10-6	reversed	1.90	1.9	1.9	4.1	5.2	7.1		12	3
10-7	reversed	2.14	2.0	2.1	3.0	6				8
10-8	reversed	2.65	1.9	2.6	3.0	4.8	6.0*		10	6, 7
8-23	one-way multiple receiver	2.15	2.0	1.9-2.2	2.4	1.9-4.	6.0*		9	3
8-24	one-way multiple receiver	2.77	2.0	3.0			6.5		6-7	4
8-25	one-way single receiver	3.54	(2.5)	3.5	(4.2)	5.4	(5.0)		8.1	5

Parentheses indicate apparent velocities. Asterisks indicate velocities used in modeling (if different from apparent velocity). All depths are in kilometers below sea level.

arc from deeper than 12 km (Figure 3) near the Talaud-Mayu Ridge to about 8 km beneath lines 8-24 and 8-25 (Figures 4 and 5). Line 8-24 shows shoaling of basement to the northeast toward the Morotai Basin, where reflection profiles show sediments to be relatively undeformed [Silver and Moore, 1978].

Refraction lines 10-4 and 10-6 (Figure 3) form nearly collinear reversed profiles parallel to the Talaud-Mayu Ridge but at an angle of about 15° to the Halmahera Thrust (Figure 2). Both 10-4 and 10-6 have well-determined solutions, but correlation between the depths and velocities for the layers shown is uncertain. The positions of the two profiles with respect to the Halmahera Thrust (line 10-4 being 30 km farther away than 10-6) and the dissimilarity between 10-4 and 10-6 express the rapid change in structure toward Halmahera. The deepest basement observed in the Molucca Sea, as inferred from refraction profiling, is apparent beneath line 10-4. Basement of velocity 6.5 km/s dips to the north at about 3° to a maximum depth of 16 km below sea level. Farther to the south, beneath line 10-6, basement shallows to 12 km below sea level and has a velocity of 7.1 km/s.

Basement velocities of 6.5 and 7.1 km/s do not correspond to average velocities observed for the top of oceanic crust in deep ocean basins [Christensen and Salisbury, 1975]. The thick collision complex is likely masking the upper oceanic crustal layer, thus causing an erroneously deep calculation for the actual top of crystalline basement. The error in depth to basement due to the masking effect is of

the order of 0.4 km for line 10-4 (assuming that an upper crustal layer 1.5 km thick and with a velocity of 5.1 km/s overlies the observed 6.5-km/s layer). The attempt to assign the observed basement velocities to specific layers within average oceanic crust is impractical because at pressures of 2.5 kbar (as is estimated for the base of the collision complex) the compressional velocities of oceanic basalts and gabbros may be elevated by as much as 0.5 km/s [Fox et al., 1973].

Refraction line 8-23 (Figure 3) yields apparent velocities similar to those of line 10-4 (2.0 km/s for the upper complex layer and 2.4 km/s for the lower layer). An offset in the travel time curve observed at buoy D is interpreted as being due to faulting at the seafloor with a throw of about 1 km. The last two shots on sonobuoy D are used to locate a basement of apparent velocity 6.0 km/s at a depth of 9 km below sea level.

The westward run of line 10-8 (Figure 6) provides evidence for a block-faulted basement seaward of the Halmahera arc. Basement arrivals in the travel time curve appear to be in three distinct linear segments of varying slope with offsets between them such that time is offset in a positive sense to the west. This pattern is interpreted as the effect of crossing fault blocks within basement successively stepped down to the west away from the Halmahera arc. The eastbound run shows no basement velocity arrivals and was only 32 km long due to extreme attenuation.

An example of the high attenuation encountered in the collision complex can be seen in the record sections of line

EASTERN MOLUCCA SEA

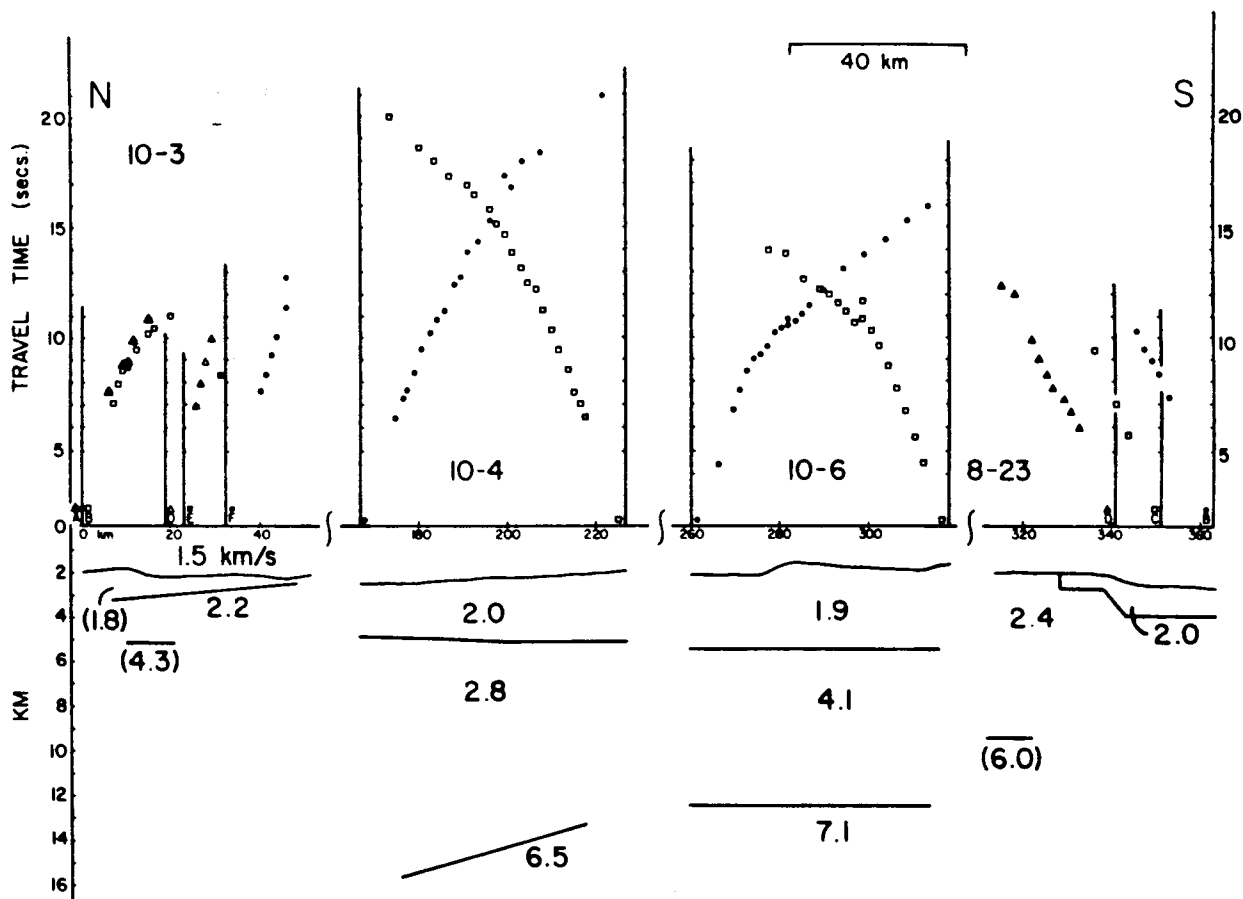


Fig. 3. North-south cross section of the Molucca Sea east of the Talaud-Mayu Ridge showing travel time curves and layer solutions for profiles shot in the north-south direction. Time axes correspond to positions of the sonobuoys, and a separate symbol is used to designate arrivals at each sonobuoy. Velocities in parentheses are assumed. Vertical exaggeration is $\times 4$.

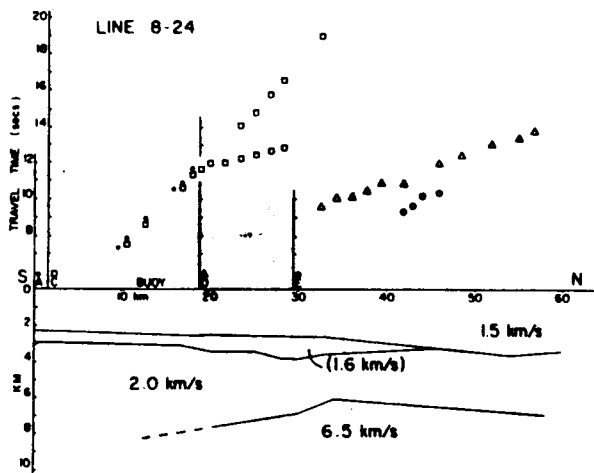


Fig. 4. Travel time curve and layer interpretation for line 8-24 northwest of Halmahera. Symbols are as in Figure 3. Vertical exaggeration is $\times 2$.

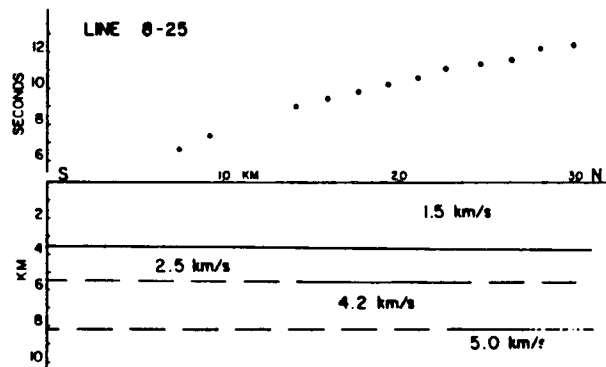


Fig. 5. Travel time curve and plane layer interpretation for line 8-25 in the Morotai Basin north of Halmahera. No vertical exaggeration.

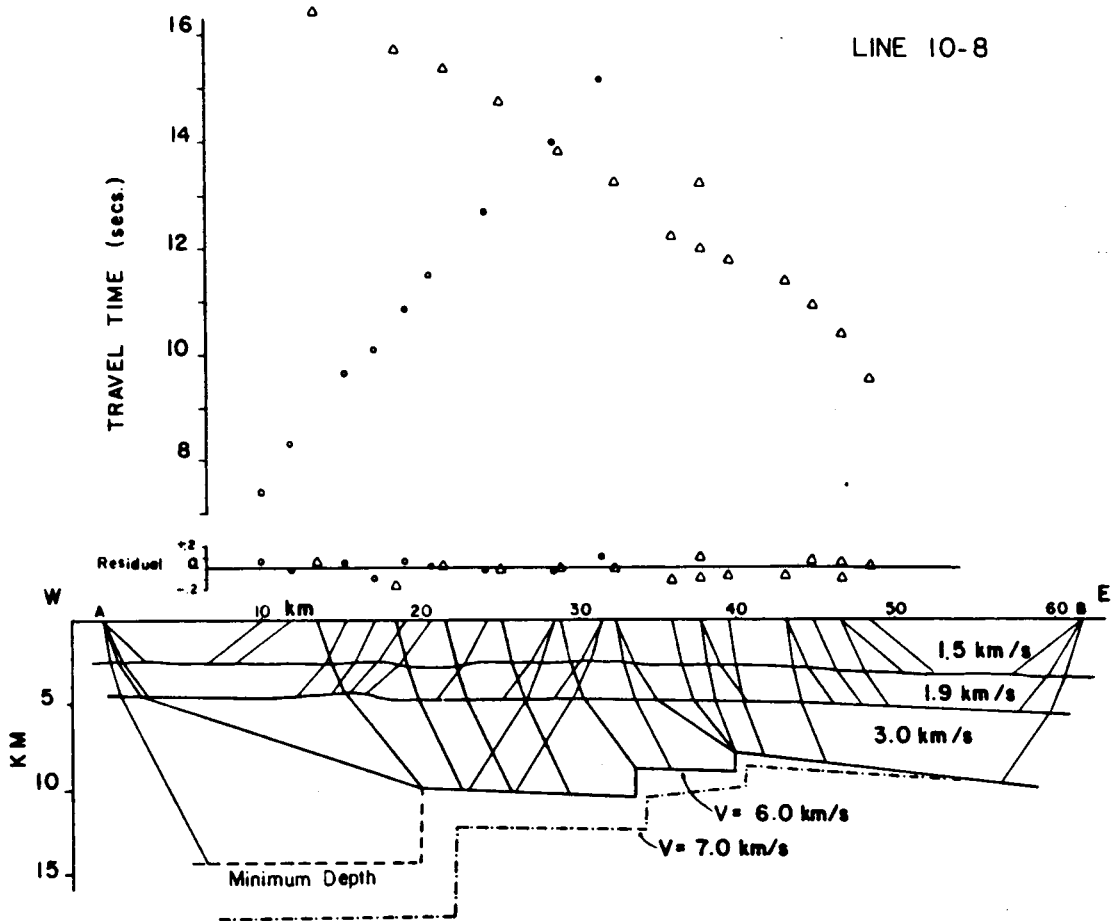


Fig. 6. Layer solution for the reversed profile 10-8 showing inferred offsets in basement downward away from the Halmahera arc. Ray paths used in the interpretation of travel time data are shown. Multiple ray paths are shown for shots near crossover distances between layers. The largest residual for this profile is 0.16 s. Basement structure is shown for two assumed basement velocities (6.0 and 7.0 km/s). A and B mark the positions of the receiving buoys. No vertical exaggeration.

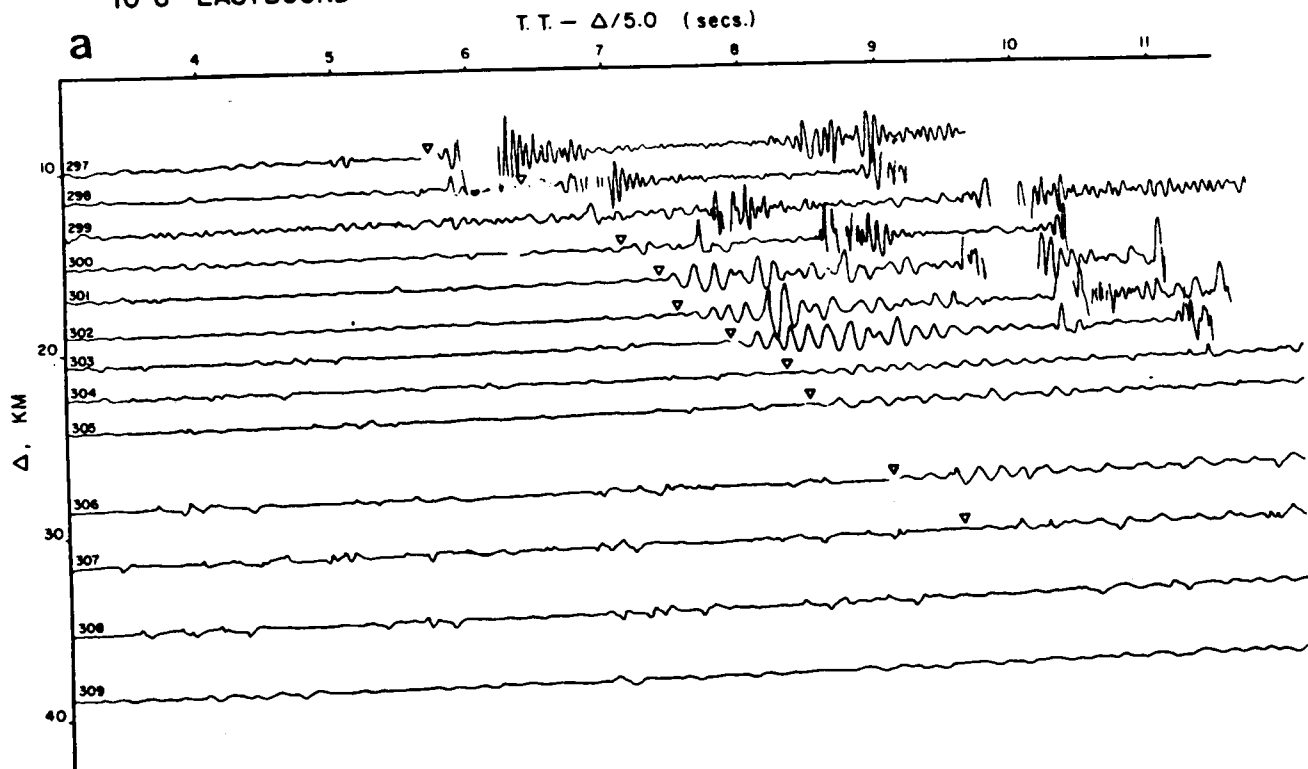
10-8 (Figure 7). Compare, for example, amplitudes of arrivals from the low- and high-velocity refractors at the same shot-to-receiver distance for the two directions of this profile. The amplitude of the basement arrival from shot 327 (10 kg of explosives) in Figure 7b is much larger than the low-velocity arrival of shot 307 (55 kg of explosives) in Figure 7a even though shot 307 is closer to the receiving buoy.

Figure 6 shows two possible basement structures for line 10-8 assuming basement velocities of 6.0 and 7.0 km/s. Lowering the assumed basement velocity in modeling necessitates a shallower basement structure but does not affect the interpretation of major crustal faulting beneath this line. First arrivals from the last two shots of the eastbound run (hypothetical ray paths shown in Figure 6) are used to calculate minimum depths to basement beneath the west side of the profile by the method of minimum

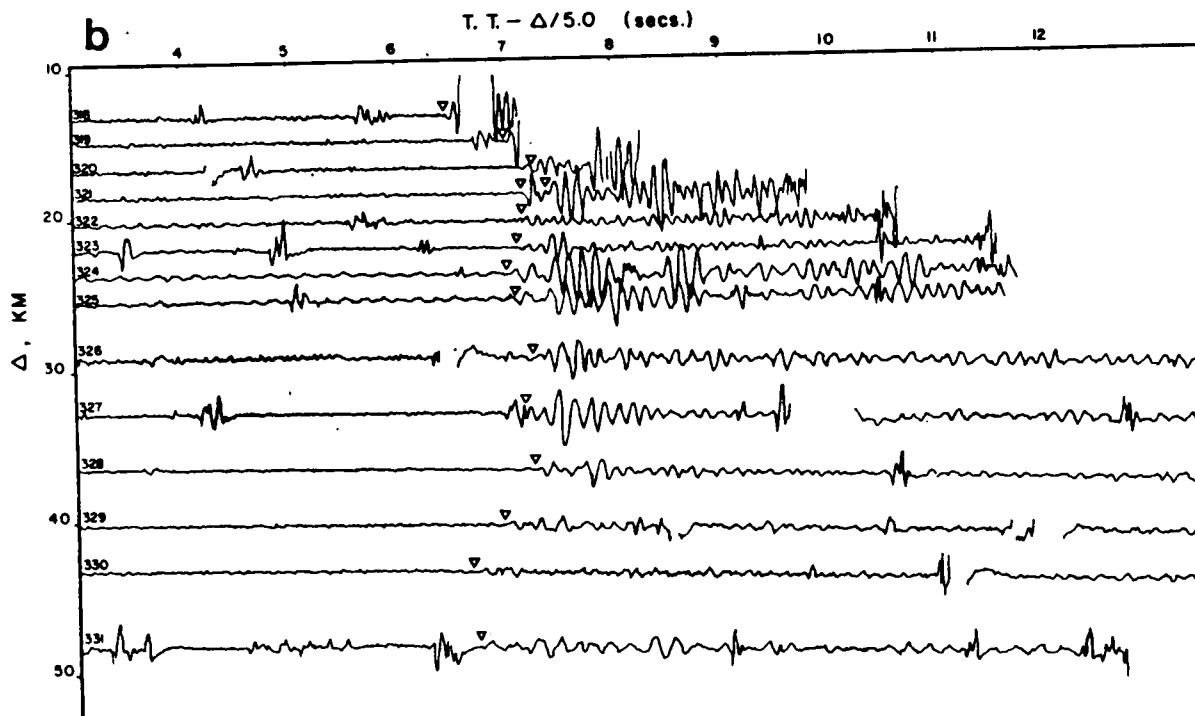
crossover distance. The lack of basement arrivals, however, cannot be considered proof that basement is deep, especially in this region of high attenuation.

Basement arrivals were observed in two refraction profiles run to the west of the Talaud-Mayu Ridge. Five arrivals with apparent velocity of 9 km/s during the southbound run of line 10-5 (Figure 8) are used to locate basement (of assumed velocity 7.0 km/s) steeply dipping to the north to a depth of 12.5 km beneath the receiving sonobuoy. The southbound and northbound runs (Figure 9) of the reversed profile 10-5 were analyzed as separate single-receiver profiles because of a lack of correlation between the two travel time curves. The large contrast between these two runs may be due to the eastward drift of about 3 km of the ship during the northbound run and may indicate rapidly changing structure in the east-west direction. At about the same latitude as 10-5 but closer to

10-8 EASTBOUND



10-8 WESTBOUND



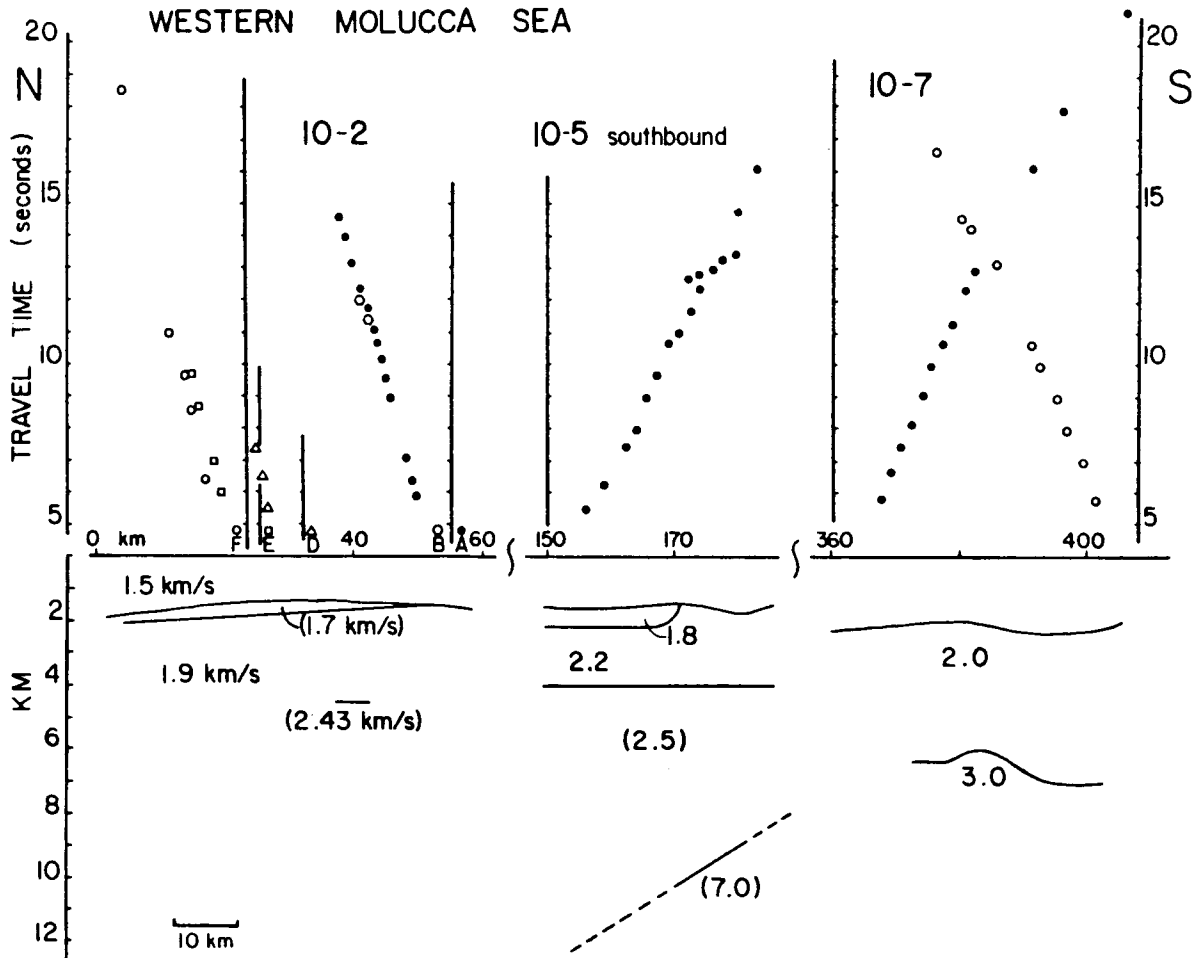


Fig. 8. North-south cross section showing travel time curves and interpretations of profiles run in the western Molucca Sea. Symbols are as in Figure 3. Vertical exaggeration is $\times 4$.

the Sangihe volcanic arc, multiple-sonobuoy line 10-1 (Figure 10) shows a 5.7-km/s basement dipping to the north at an angle of 2.8° . This refractor was followed to a maximum depth of about 9 km below sea level before refractions became unrecognizable. The velocity of this base-

Fig. 7. (Opposite) Record sections for the (a) east-bound and (b) westbound runs of reversed profile 10-8 plotted in reduced time (reducing velocity is 5.0 km/s), with topographic corrections applied. Small triangles mark onset time of refracted energy. The sharp blips on the traces which in some cases precede the picked refracted arrivals are either noise, direct waves, or seafloor reflections. Refracted energy is usually of lower frequency and is discriminated by comparing traces from filtered signals passed through high- and low-frequency bandpass filters.

ment refractor is typical of upper island arc crust and may indicate that island arc basement underlies the collision complex seaward of the present Sulawesi-Sangihe Trench (Figure 2). This is consistent with interpretations from seismic reflection profiles indicating the collision complex being overthrust onto the island arc apron in this area [Silver and Moore, 1978; Hamilton, 1979].

Refraction profiles 10-1, 10-5, and 10-4 all suggest that basement underlying the Molucca Sea dips toward the north. No basement arrivals were observed in lines 10-2 (Figure 8) or 10-3 (Figure 3) in the northern Molucca Sea, presumably as a consequence of this northward thickening of the collision complex. Gravity measurements by Vening-Meinesz [1948] show a sharp decrease in the isostatic anomaly toward the central part of the Molucca Sea in the vicinity of lines 10-2 and 10-3, where a value of less than -200 mGal is reached. Basement depths of 17 km below sea level overlain by a thick, low-density collision complex can

LINE 10-5 NORTHBOUND

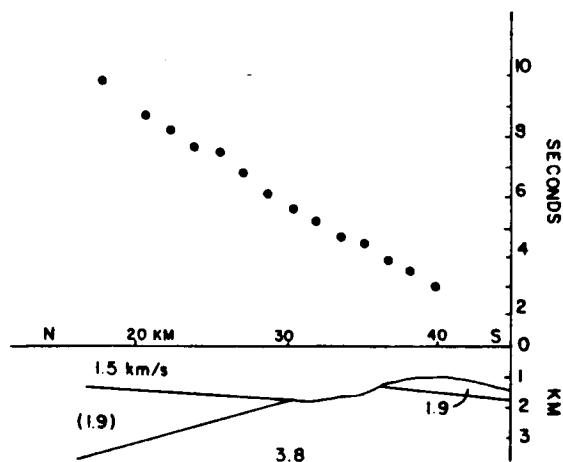


Fig. 9. Layer solution for the northbound run of line 10-5. Vertical exaggeration is $\times 2$.

account for this low gravity value, and such a large thickness of highly attenuating melange may also explain the lack of recognizable basement arrivals in lines 10-2 and 10-3. Farther to the south, line 10-7 (Figure 8) proved unsuccessful in penetrating the collision complex, but an estimate for the minimum depth to a basement of 6.0 km/s is 17.4 km below sea level.

Gravity Interpretation

The interpretation of these refraction profiles in conjunction with two long free air gravity profiles constrains models for the crustal structure of the Molucca Sea collision zone. The southern traverse (Figure 2) extends from the Gorontalo Basin eastward to the southern tip of Halmahera, and the central traverse crosses the Molucca Sea from North Arm, Sulawesi, to north central Halmahera.

Densities within the collision complex are approximated from measured seismic velocities using the conversion curve of *Nafe and Drake* [1963]. The average crustal density is taken to be 2.86 g/cm³ to a depth of 32 km below sea level, and an upper mantle density of 3.3 g/cm³ is assumed [Ringwood, 1969]. Bathymetry is controlled by underway 12-kHz echo sounding, and the accuracy of the free air gravity measurements is estimated to be 5 mGal. The gravity effects for trial models are computed using the two-dimensional modeling algorithm of *Talwani et al.* [1959].

The southern traverse (Figure 11) is constrained by refraction lines 10-7 and 10-8, which run perpendicular to and parallel to the gravity profile, respectively. The basement structure calculated assuming a basement velocity of 6.0 km/s beneath line 10-8 is used in the gravity model, and a minimum depth to basement of 17.4 km constrains the model beneath 10-7.

LINE 10-1

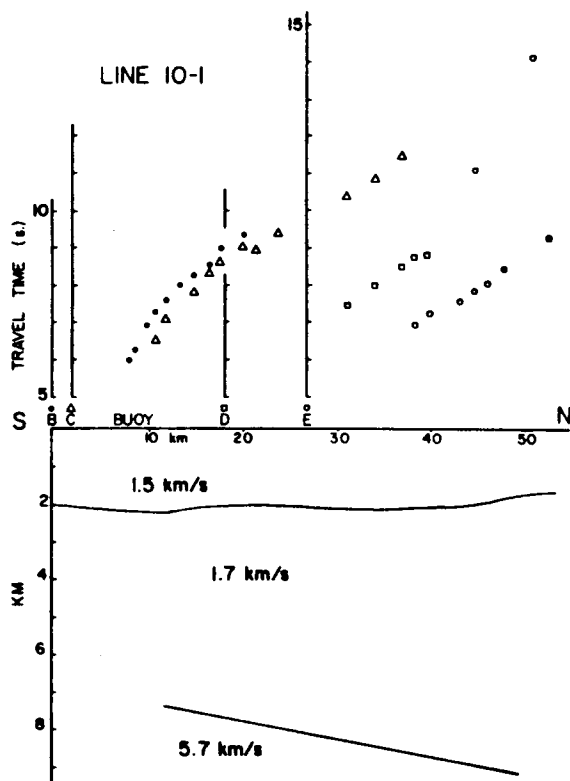


Fig. 10. Plane layer interpretation for line 10-1. Symbols are as in Figure 3. Vertical exaggeration is $\times 4$.

The gravity field over the southern Molucca Sea is well modeled by a very thick, low-density wedge of material overlying oceanic crust. The symmetry of the gravity field is broken by a local high above the Talaud-Mayu Ridge, to the east of the gravity minimum. This high is not due to the topographic effect of the ridge alone. We have interpreted this high as being caused by a slice of high-density material steeply inclined beneath the Talaud-Mayu Ridge. The asymmetric shape of the local anomaly over the Talaud-Mayu Ridge with a steeper gradient to the west suggests an eastward dip for the mass excess as shown in Figure 11.

On the east and west sides of the Molucca Sea the trenches have little effect on the observed gravity field, although they are 1.5-2.0 km deeper than the average depth in the basin. In order to keep the calculated gravity curves from having local minima over the trenches in our models, we show the crust-mantle boundary shallowing slightly beneath the trenches before descending beneath the island arcs. This arcward shallowing of the mantle gives the appearance of downward buckling of the crust in the Molucca Sea. The surface expression of a synformal structure is seen in a reflection profile just west of this traverse [Silver and Moore, 1978, Figure 11] in which undeformed sedi-

LINE 10-5 NORTHBOUND

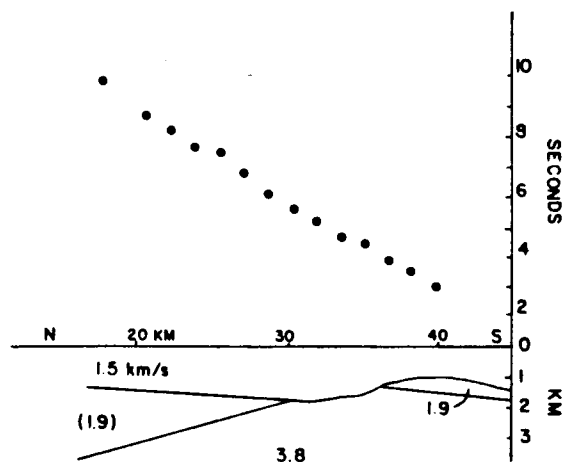


Fig. 9. Layer solution for the northbound run of line 10-5. Vertical exaggeration is $\times 2$.

account for this low gravity value, and such a large thickness of highly attenuating melange may also explain the lack of recognizable basement arrivals in lines 10-2 and 10-3. Farther to the south, line 10-7 (Figure 8) proved unsuccessful in penetrating the collision complex, but an estimate for the minimum depth to a basement of 6.0 km/s is 17.4 km below sea level.

Gravity Interpretation

The interpretation of these refraction profiles in conjunction with two long free air gravity profiles constrains models for the crustal structure of the Molucca Sea collision zone. The southern traverse (Figure 2) extends from the Gorontalo Basin eastward to the southern tip of Halmahera, and the central traverse crosses the Molucca Sea from North Arm, Sulawesi, to north central Halmahera.

Densities within the collision complex are approximated from measured seismic velocities using the conversion curve of *Nafe and Drake* [1963]. The average crustal density is taken to be 2.86 g/cm³ to a depth of 32 km below sea level, and an upper mantle density of 3.3 g/cm³ is assumed [Ringwood, 1969]. Bathymetry is controlled by underway 12-kHz echo sounding, and the accuracy of the free air gravity measurements is estimated to be 5 mGal. The gravity effects for trial models are computed using the two-dimensional modeling algorithm of *Talwani et al.* [1959].

The southern traverse (Figure 11) is constrained by refraction lines 10-7 and 10-8, which run perpendicular to and parallel to the gravity profile, respectively. The basement structure calculated assuming a basement velocity of 6.0 km/s beneath line 10-8 is used in the gravity model, and a minimum depth to basement of 17.4 km constrains the model beneath 10-7.

LINE 10-1

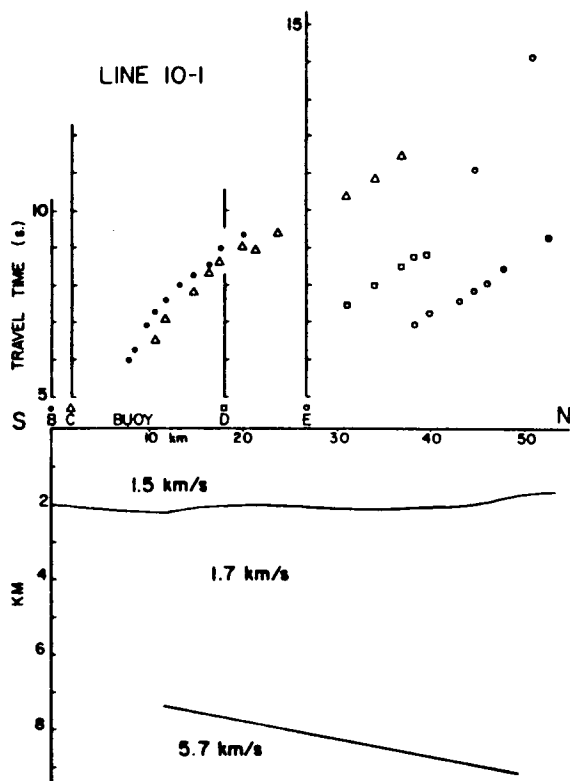


Fig. 10. Plane layer interpretation for line 10-1. Symbols are as in Figure 3. Vertical exaggeration is $\times 4$.

The gravity field over the southern Molucca Sea is well modeled by a very thick, low-density wedge of material overlying oceanic crust. The symmetry of the gravity field is broken by a local high above the Talaud-Mayu Ridge, to the east of the gravity minimum. This high is not due to the topographic effect of the ridge alone. We have interpreted this high as being caused by a slice of high-density material steeply inclined beneath the Talaud-Mayu Ridge. The asymmetric shape of the local anomaly over the Talaud-Mayu Ridge with a steeper gradient to the west suggests an eastward dip for the mass excess as shown in Figure 11.

On the east and west sides of the Molucca Sea the trenches have little effect on the observed gravity field, although they are 1.5–2.0 km deeper than the average depth in the basin. In order to keep the calculated gravity curves from having local minima over the trenches in our models, we show the crust-mantle boundary shallowing slightly beneath the trenches before descending beneath the island arcs. This arcward shallowing of the mantle gives the appearance of downward buckling of the crust in the Molucca Sea. The surface expression of a synformal structure is seen in a reflection profile just west of this traverse [Silver and Moore, 1978, Figure 11] in which undeformed sedi-

SOUTHERN MOLUCCA SEA

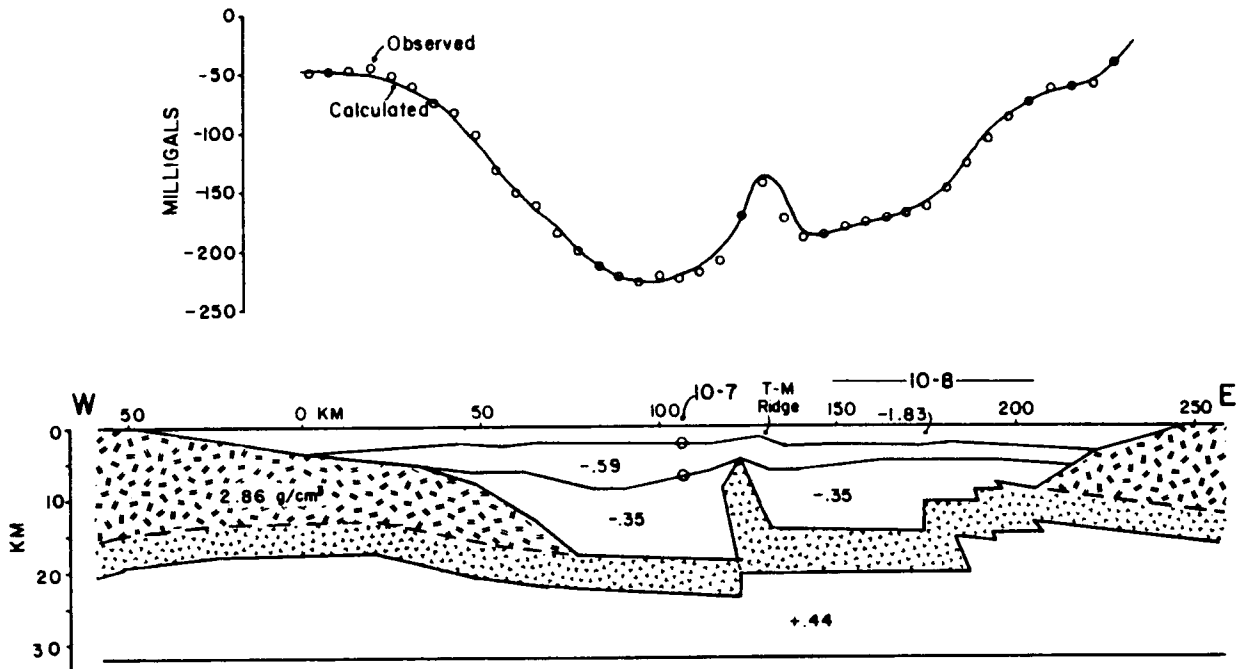


Fig. 11. Gravity profile and crustal model satisfying refraction and gravity data in the southern Molucca Sea. Layers in the crustal model are designated by their density contrasts with an assumed crustal density of 2.86 g/cm^3 . Refraction control points are shown by open circles on interfaces beneath 10-7, and structure beneath 10-8 is as shown in Figure 6 for the 6.0-km/s basement described in the text. Vertical exaggeration is $\times 2$. The small v pattern represents oceanic crust, and island arc crust is designated by a short parallel line pattern.

ments on the arc apron are tilted slightly toward the Molucca Sea. The weight of the thick overlying collision complex may be effectively depressing the crust of both the island arcs and the Molucca Sea plate.

In the central Molucca Sea (Figure 12) the gravity profile is similar in shape to the southern profile, with the notable exception that for the central line the local high is to the west of the minimum value and much broader than it is in the southern traverse. A more significant difference is that the entire curve seems to be shifted in a positive sense by about 100 mGal in going from the south to the central traverse. The minima are -130 mGal (central) and -230 mGal (southern), which increase toward the island arcs and approach values of 100 mGal (central) and 0 mGal (southern) toward the ends of the respective profiles. Thus we feel that a large part of this difference of 100 mGal between the central and southern traverses has a deeper or broader source than the low-density collision complex.

Grow and Bowin [1975] analyzed a gravity transect, constrained by refraction studies, across the Chile Trench and concluded that the contribution to the gravity field

from the sinking slab must be about 100 mGal in the vicinity of the trench axis. The central profile (Figure 12) lies in an area above well-documented lithospheric slabs within the asthenosphere [Cardwell *et al.*, this volume]. The southern profile is to the south of the southernmost extent of these subducted slabs. Assuming a density contrast of 0.05 g/cm^3 between asthenosphere and the more dense, subducted lithosphere beneath the Sangihe and Halmahera island arcs, the difference in regional gravity between the central and southern profiles due to subducted slabs is approximately 60-70 mGal (as determined by three-dimensional gravity modeling). The southern traverse lies near the Banggai-Sula Islands (Figure 1), over which there is a narrow, positive ($+200 \text{ mGal}$) free air anomaly [Watts *et al.*, 1978]. The source of the anomaly over the Banggai-Sula Islands is presumably at crustal depths and has a small (less than 10 mGal) but positive effect on the observed gravity of the southern traverse.

Figure 12b shows a gravity model for the mantle structure, which we suggest as a possible source of part of the 100-mGal difference between the south and central Molucca Sea. The structure shown, a modified version of the

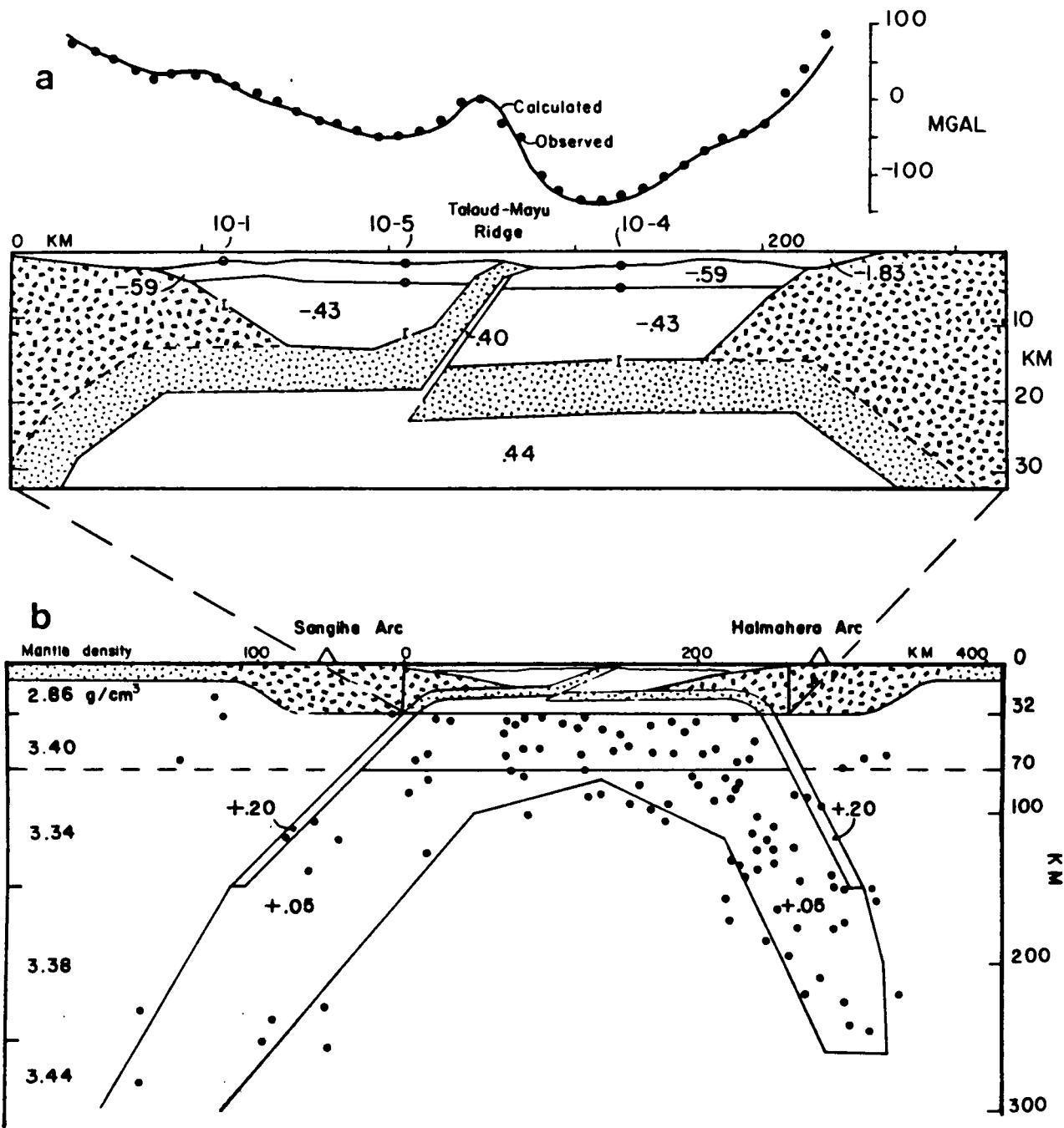


Fig. 12. Gravity model for the central Molucca Sea. (a) Crustal model with layers designated by their density contrasts and refraction control points by open circles and vertical bars. (b) Mantle structure used in modeling the gravity profiles in the central Molucca Sea. Figure 12a fits into the small box at the apex of the inverted-V-shaped lithosphere. Slab dimensions are controlled by earthquake foci (dots) from *Hatherton and Dickinson* [1969], and mantle densities are taken from *Grow and Bowin* [1975]. The column at the left shows assumed densities for the range of depths between the tick marks. The small v pattern represents oceanic crust, and island arc crust is designated by a short parallel line pattern. East is to the right of the figure.

model of *Grow and Bowin* [1975], has an effect of about 80 mGal over the length of the profile and is used only to account for regional effects in modeling the central traverse. This structure represents an inferred source of the regional field in the central Molucca Sea and, owing to the fact that it does not underlie the southern Molucca Sea, is not considered a significant contributor to the regional field in the vicinity of the southern gravity profile. Part of the difference between the central and southern gravity profiles may be due to changes in collision complex thickness.

The central gravity traverse (Figure 12a) is constrained by refraction lines 10-4, 10-5 and 10-1. All of these lines revealed a northward dipping basement refractor, and because of uncertainty as to whether these depths represent the actual top of the underlying crust, we have constrained basement depths in the gravity models only to within 0.5 km above or below the depths calculated from the refraction profiles.

We interpret the shallowing of basement from east to west across the Molucca Sea as being due to major reverse faulting within the Molucca Sea plate beneath the Talaud-Mayu Ridge. Earthquake maps of the Molucca Sea [e.g., *Hamilton*, 1974] show a high density of earthquake epicenters diffusely distributed along the Talaud-Mayu Ridge, and the predominant mechanism is thrust type [*Fitch*, 1970, 1972; *Fitch and Molnar*, 1970; *Cardwell et al.*, this volume]. Preliminary results from a recent local earthquake survey (R. McCaffrey, unpublished data, 1978) indicate that this activity is mostly between 20- and 60-km depth and may be confined to discrete zones.

The local free air gravity high over the Talaud-Mayu Ridge in the central region of the Molucca Sea is much broader and of higher amplitude (approximately 40 mGal higher) than that to the south. We similarly interpret this local high to be due to a steeply dipping high-density body, though much more high density material is needed in the central Molucca Sea to match the observed gravity. The presence of peridotite and gabbro on the island of Mayu, located 30 km south of this profile, provides the requisite high-density material and suggests incorporation of fragments of the overridden Molucca Sea plate into the central zone of the collision complex. The strongly symmetric shape of the local Bouguer anomaly (regional trend and topographic effect of ridge removed) above this ridge suggests that the mass excess is very steeply inclined beneath and fairly symmetrically distributed with respect to the Talaud-Mayu Ridge. Figure 13 shows three possible models for the internal structure of the Talaud-Mayu Ridge. Figure 13a is the same structure as that in Figure 12a, in which a single slice of oceanic crust including a slab of upper mantle material 1 km thick is assumed to form the root of the Talaud-Mayu Ridge. In Figure 13b, slices of oceanic crust act to thicken the crust tectonically, and Figure 13c is similar to Figure 13a, except an eastward dip is assumed for the high-density sliver.

Brief field observations on Mayu Island by R.

McCaffrey and E. A. Silver revealed that the dominant rock type changes from mafic to ultramafic eastward across the island, which is 8 km wide. This apparent distribution of gabbro and peridotite on Mayu favors the orientation of east vergence shown in Figures 12a, 13a, and 13b. The intense seismicity between the island arcs may be associated, in part, with the upward thrusting of this high-density slab.

Velocity Structure of the Collision Complex

Refraction studies conducted in the Molucca Sea collision zone have revealed, by constant velocity layer assumptions, a distinct difference in the variability of measured velocities (excluding masked layers) between the apparent upper and lower layers of the collision complex (Table 1). The upper layer is apparently quite consistent in velocities (ranging from 1.7 to 2.2 km/s, centered at 2.0 km/s for 11 determinations) and in depth to its base (4-6 km below sea level for all but two cases). The lower 'layer' of the collision complex, on the other hand, is quite variable in velocities, ranging from 2.4 to 4.1 km/s with a mean of about 3.1 km/s (for seven velocity determinations). This contrast in variability of velocities between the two layers is due in part to the rapid decrease in the accuracy of picking arrivals with increasing range and the fact that higher velocities (as determined from the travel time curve) are more sensitive to small changes in travel times than are lower velocities.

The interpretation of seismic refraction profiles in terms of constant velocity layers is not proof that such discrete layers exist. Experimental errors of 0.1 s, shot spacings of at least 1 km, and poor resolution of second arrivals in these profiles allow a large family of velocity-depth solutions of which the plane layer solution is only one member. We have presented solutions in terms of a finite number of constant velocity layers for the sake of clarity.

Actual velocity likely varies in a more continuous manner with depth in the collision complex. As a first approximation to the case of a continuous increase in velocity with depth within the collision complex, we have determined linear velocity-depth solutions using only refracted arrivals from the collision complex. If velocity is a linear function of depth only, then the observed travel time T is given by

$$T = \frac{2}{k} \sinh^{-1} \left(\frac{kX}{2V_0} \right) + t + e$$

[*Dobrin*, 1976], where k is the vertical velocity gradient, X is the shot-detector distance, and V_0 is the surface velocity. The time axis intercept t will be nonzero in the case of a constant velocity layer overlying the section in which velocity increases linearly with depth. The value of t will vary with the ray parameter, but t is small for these profiles (less than 0.5 s), and we have considered it constant from shot to shot within each profile. All shots and receivers were reduced to the seafloor datum, and k was deter-

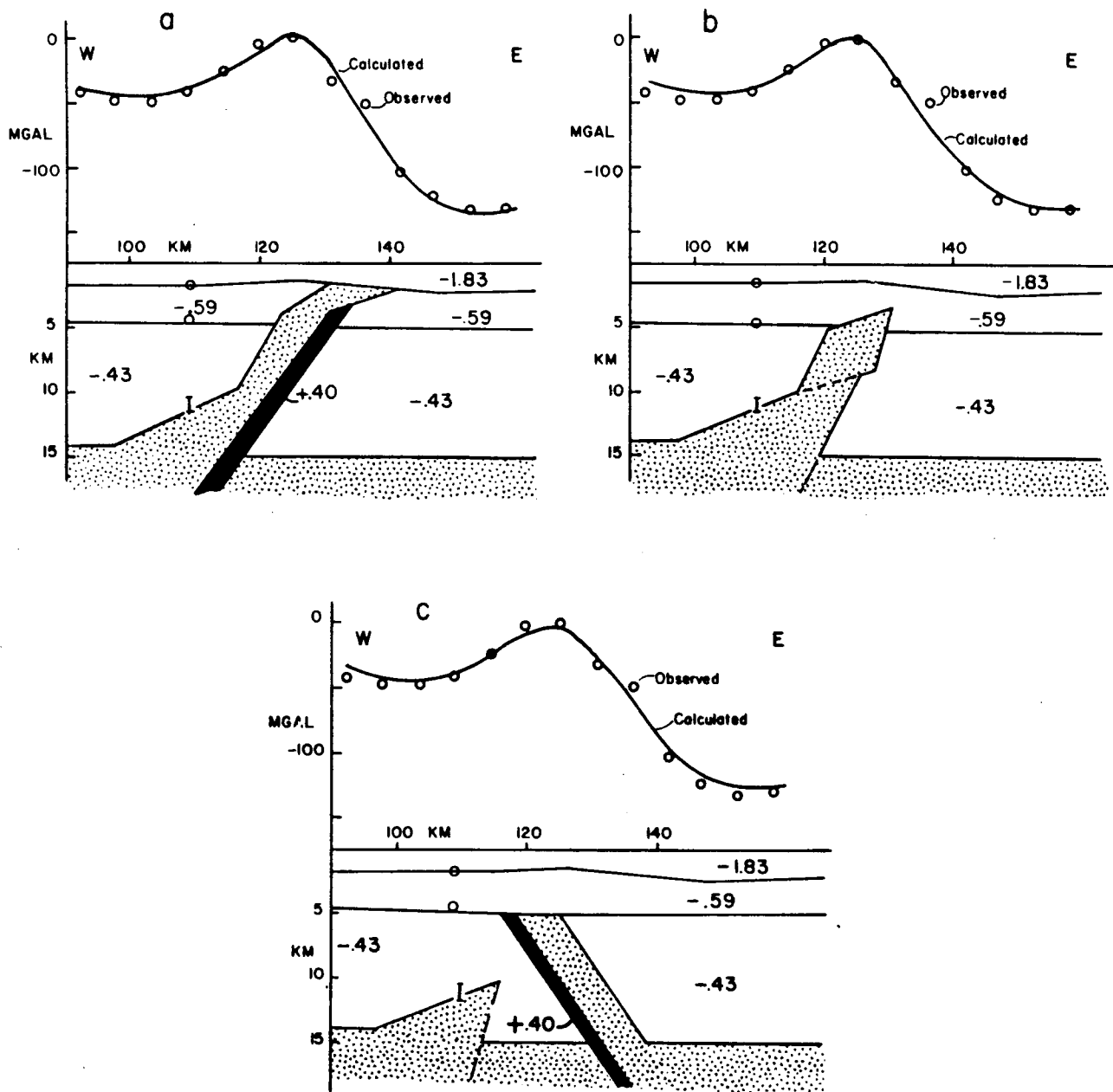


Fig. 13. Representative models for internal structure of the Talaud-Mayu Ridge. Numbers within layers indicate density contrast (with respect to assumed average crustal density of 2.86 g/cm^3). Horizontal distances given correspond to those of Figure 12. Darkened layer is assumed to be mantle density material, and small v pattern represents oceanic crust. Circles and bars represent control points taken from refraction line 10-5.

mined by minimizing the sum of the squares of the residuals (e).

Five out of nine values for k determined for collision complex refractions fall within the range 0.10–0.17 km/s per kilometer depth. A mean gradient for all collision com-

plex arrivals (except those of line 10-6 which display a rapid increase in velocity with depth, $k=0.34$) is 0.14 km/s per kilometer and represents a surprisingly good fit (rms error of 0.29 s). This value of k seems to be a reasonable estimate for the general increase in velocity with depth in

the collision complex. Laboratory pressure-velocity relations determined by *Schreiber et al.* [1972] for semi-indurated sediments indicate a rate of change of compressional velocity with pressure of about 0.2 km/s per kilobar pressure (for pressures less than 2.5 kbar). Assuming a constant sediment density of 2.5 g/cm³, the contribution to k from an increase in pressure with depth is 0.05 km/s per kilometer. Other depth-dependent factors such as cementation and water content may make up a significant portion of the observed value for k .

Actual velocity discontinuities may nevertheless exist within the collision complex. Irregularities in travel time curves may be indicative of blocks with significant velocity contrasts included within the collision complex. The detection of higher apparent velocity arrivals at buoy A of line 10-2 (Figure 8) and buoy B of line 10-3 (Figure 3), which did not appear at any of the other sonobuoys of these profiles though critical distances were exceeded, may indicate an interface of limited lateral extent (or steeply dipping). Lines 10-5N (Figure 9) and 8-23 (Figure 3) display sharp lateral velocity discontinuities within the uppermost part of the collision complex. The irregularity of the travel times at the scale of a few shots and the overall similarity in travel time curves from profile to profile lead us to conclude that the seismic structure of the collision complex is dominated by velocity gradients, possibly due to compaction with depth and cementation but complicated by included blocks as large as several tens of kilometers.

Discussion

Seismic refraction and gravity profiles from the Molucca Sea of eastern Indonesia serve to further delineate crustal structure produced by this active arc-arc collision. The collision between the facing Sangihe and Halmahera island arcs has trapped a volumetrically enormous symmetric wedge of low-density material, presumably the amalgamation of subduction complexes associated with the individual arcs prior to collision. Land masses presently surrounding the Molucca Sea are small and are precluded as major sources of sediment. *Hamilton* [1979] suggests New Guinea as an origin of abundant sediment for the Halmahera Trench when this arc was east of its present position.

The immense thickness and weight of the collision complex appears to depress the crust of the buried Molucca Sea plate beneath the Talaud-Mayu Ridge. Reorientation of stress axes within the upper part of the Molucca Sea plate by crustal loading may be responsible in part for the apparent state of horizontal compression as inferred by focal mechanism solutions. Flexural compressive stresses within the upper part of a 60-km-thick plate under a rapidly applied (approximately 1 m.y.) line load will exceed the crushing strength of rock after vertical displacement of only 1 km [*Walcott*, 1976]. The collision complex is over 700 km long, 100-150 km wide, and up to 15 km thick and can therefore be approximated by a line load on the underlying Molucca Sea lithosphere. Assuming the densities and geometries shown in Figures 11 and 12 and the load-dis-

placement relationship of *Walcott* [1976], the thickness of collision complex required to produce a 1-km vertical displacement of the underlying lithosphere is 4 km for an unbroken plate. Seismic refraction profiles have shown the collision complex to be 3-4 times the thickness necessary, by this analysis, to induce crustal failure.

The transformation of the Molucca Sea lithosphere from an originally concave down to a concave up configuration, as is shown in Figure 11, can account for a considerable degree of horizontal shortening within the crustal layers. The total amount of crustal shortening (4%) shown in Figure 11 can be produced by simple synclinal bending of a 70-km-thick lithospheric plate from its original radius of curvature (the radius of the earth) to a final radius of curvature of about 1000 km. The radius of curvature for the downbowing of crust beneath the Talaud-Mayu Ridge along the southern gravity traverse is estimated at 700 km. Following initial failure of the buried plate, continued convergence may be taken up largely by thrusting along the central ridge rather than along the margins of the collision zone near the volcanic arcs.

Appendix

Refraction profiles presented in this paper were run during the INDOPAC Expedition, legs 8 and 10, as part of a continuing geophysical investigation of the Molucca Sea collision zone. Gravity profiles were obtained during leg 7 in August 1976. All refraction profiles were single-ship lines employing either moored sonobuoys (one at each end of the reversed profiles) or multiple drifting sonobuoys deployed intermittently over the length of the profile.

All profiles were solved initially by an undulating layer solution method [*Raitt et al.*, 1969], which matches the observed travel time curve with the best fit refracting interfaces whose depths are polynomial or Fourier series functions of position. This method gave good fits for some of the observed travel time curves (10-1, 10-2, 10-3, 10-6, and 8-25) with rms errors typically of 0.2 s. Standard corrections were applied to the travel times of these profiles as described by *Shor* [1963].

Several of the travel time curves, however, exhibit a degree of complexity which makes plane layer solutions inapplicable. In best fitting straight lines to segments of some of the travel time curves we found residuals as large as 0.6 s. Such large residuals must be construed as being produced by significant structural deviations from planar layers. In order to incorporate anomalous travel times (with respect to smooth layer assumptions) into models, we have solved the profiles by a process of tracing rays through trial models while adjusting the models to fit the observed travel times. In this way we require the structural and velocity model to satisfy the observed travel time curve (within estimated error) rather than smoothing the travel time curve to fit one of a family of predetermined models. The rms errors for solutions by the ray-tracing method are one-half to one-third those of plane or undulating layer solutions for reversed profiles

(which offer a better test to degree of fit than do one-way profiles). Lines 10-4, 10-5N, 10-5S, 10-7, 10-8, 8-23, and 8-24 were modeled in this way, and Figure 6 gives an example of ray paths used.

Total accuracy of the refraction experiment is taken to be 0.10 s, and this is considered to be a good fit in the modeling process. Bathymetry is incorporated into the models in the form of two-way travel time through the water layer, and this is known to be better than 0.01 s. Water depths are taken from 3.5- and 12-kHz Giffit depth recorders which assume a two-way vertical velocity of 400 fathoms (0.75 km) per second in the water layer. The depth values are converted to one-way travel times and then to kilometers by using an average water velocity of 1.50 km/s (very close to the average sounding velocity for 2- to 3-km depth as determined from expendable bathythermograph data taken at each profile and nearby hydrographic data from leg 7). These depth values and this velocity are used in the ray-tracing process. Variations in the water velocity with depth introduce a small error in the bathymetry used in the models, but this amounts to no more than 1.5% of the water depth in the range of 2- to 3-km depth.

Firing time corrections are made to within 0.01 s [Shor, 1963]. The largest error is picking the actual time of arrival of the refracted energy from the record, and this error is estimated at 0.08 s for these profiles in the Molucca Sea, where high-frequency components of the energy traveling through the collision complex are attenuated considerably over short distances. The pick of arrival time decreases in accuracy with increasing shot-detector distance, and this effect was considered in modeling the more distant shots.

Errors in calculating travel times for trial models in the ray-tracing process are much less than those of the refraction method. The sources of error are in measuring ray lengths and angles. The largest time error for a single layer will be in the water layer because of its low velocity, and for the scale used in modeling these profiles (2.5 cm (1 inch) per kilometer), this error is of the order of 0.013 s. If all measurement errors were of the same sign (and we have no reason to expect such a preference), a four-layer model such as is interpreted for line 10-4 would have a maximum error of 0.064 s. The sum of the errors from all layers would tend to zero if the signs were evenly distributed. An error of 1° in the critical angle produces a maximum error of +0.002 s per interface for the range of layer thicknesses and velocities presented in this study.

Shot-detector distances were calculated by using direct water wave time and the seismic velocity in the water layer as determined from bathythermograph and hydrocast data. In the longer profiles the direct wave was not received at great distances, in which case bottom reflections were used to calculate range.

Acknowledgments. We thank A. Arsenault and crew and scientific party of the R/V *Thomas Washington* for

their cooperation during leg 10 of the INDOPAC Expedition. P. O'Neill, R. M. Kieckhefer, S. Smith, and M. Wolfe were instrumental in shipboard operations, and D. McGowan was quite helpful in data reduction. We also thank G. Shor for arranging ship time and for providing refraction profiles from INDOPAC leg 8. R. M. Kieckhefer, W. Hamilton, and R. Cardwell offered valuable suggestions on the manuscript. This work was supported by the National Science Foundation, grant OCE76-81880.

References

- Cardwell, R. K., B. L. Isacks, and D. E. Karig, The spatial distribution of earthquakes, focal mechanism solutions and plate boundaries in the Philippine and northeastern Indonesian islands, this volume.
- Christensen, N. I., and M. H. Salisbury, Structure and constitution of the lower oceanic crust, *Rev. Geophys. Space Phys.*, **13**, 57-86, 1975.
- Dewey, J. F., and J. M. Bird, Mountain belts and the new global tectonics, *J. Geophys. Res.*, **75**, 2625-2647, 1970.
- Dobrin, M., *Introduction to Geophysical Prospecting*, 3rd ed., 630 pp., McGraw-Hill, New York, 1976.
- Fitch, T. J., Earthquake mechanisms and island-arc tectonics in the Indonesian-Philippine region, *Bull. Seismol. Soc. Amer.*, **60**, 565-591, 1970.
- Fitch, T. J., Plate convergence, transcurrent faults and internal deformation adjacent to southeast Asia and the western Pacific, *J. Geophys. Res.*, **77**, 4432-4460, 1972.
- Fitch, T. J., and P. Molnar, Focal mechanisms along inclined earthquake zones in the Indonesian-Philippine region, *J. Geophys. Res.*, **75**, 1431-1444, 1970.
- Fox, P. J., E. Schreiber, and J. J. Peterson, The geology of the oceanic crust: Compressional wave velocities of oceanic rocks, *J. Geophys. Res.*, **78**, 5155-5172, 1973.
- Grow, J. A., and C. O. Bowin, Evidence for high-density crust and mantle beneath the Chile trench due to the descending lithosphere, *J. Geophys. Res.*, **80**, 1449-1458, 1975.
- Hamilton, W., Earthquake map of the Indonesian region, *Misc. Invest. Map Ser. I-875-C*, U. S. Geol. Surv., Reston, Va., 1974.
- Hamilton, W., Tectonics of the Indonesian region, *U.S. Geol. Surv. Prof. Pap.*, **1078**, 345 pp., 1979.
- Hatherton, T., and W. R. Dickinson, The relationship between andesitic volcanism and seismicity in Indonesia, the Lesser Antilles, and other island-arcs, *J. Geophys. Res.*, **74**, 5301-5310, 1969.
- Mammerickx, J., R. L. Fisher, F. J. Emmel, and S. M. Smith, Bathymetry of the east and southeast Asian seas, *Map and Chart Ser. MC-17*, Geol. Soc. of Amer., Boulder, Colo., 1976.
- McKenzie, D. P., Speculations on the consequences and causes of plate motions, *Geophys. J. Roy. Astron. Soc.*, **18**, 1-32, 1969.
- Nafe, J. E., and C. L. Drake, Physical properties of marine

- sediments, in *The Sea*, vol. 3, edited by M. N. Hill, pp. 794-815, John Wiley, New York, 1963.
- Raiff, R. W., The crustal rocks, in *The Sea*, vol. 3, edited by M. N. Hill, pp. 85-102, John Wiley, New York, 1963.
- Raiff, R. W., G. G. Shor, T. J. G. Francis, and G. B. Morris, Anisotropy of the Pacific upper mantle, *J. Geophys. Res.*, **74**, 3095, 1969.
- Ringwood, A. E., Composition and evolution of the upper mantle, in *The Earth's Crust and Upper Mantle*, *Geophys. Monogr. Ser.*, vol. 13, edited by P. J. Hart, pp. 1-17, AGU, Washington, D. C., 1969.
- Schreiber, E., P. J. Fox, and J. J. Peterson, Compressional sound velocities in semi-indurated sediments and basalts from DSDP leg II, in *Initial Reports of the Deep-Sea Drilling Project*, vol. 11, p. 723, U.S. Government Printing Office, Washington, D. C., 1972.
- Shor, G. G., Refraction and reflection techniques and procedure, in *The Sea*, vol. 3, edited by M. N. Hill, pp. 20-38, John Wiley, New York, 1963.
- Silver, E. A., A new tectonic map of the Molucca Sea and East Sulawesi, Indonesia, with implications for hydrocarbon potential and metallogenesis, paper presented at the Ad Hoc Working Group Meeting on the Geology and Tectonics of Eastern Indonesia, Stud. of East Asian Transect and Resour., Bandung, Indonesia, July 9-14, 1979.
- Silver, E. A., and J. C. Moore, The Molucca Sea collision zone, Indonesia, *J. Geophys. Res.*, **83**, 1681-1691, 1978.
- Sukanto, R., Tectonic significance of melange of the Talaud Islands, northeastern Indonesia, paper presented at the Ad Hoc Working Group Meeting on the Geology and Tectonics of Eastern Indonesia, Stud. of East Asian Transect and Resour., Bandung, Indonesia, July 9-14, 1979.
- Talwani, M., J. L. Worzel, and M. Landisman, Rapid gravity computations for the two-dimensional bodies with application to the Mendocino submarine fracture zone, *J. Geophys. Res.*, **64**, 49, 1959.
- Vening-Meinesz, F. A., *Gravity Expeditions at Sea, 1923-1938*, vol. 4, 233 pp., Delftshe, Uitgevers Maatschappij Delft, Netherlands, 1948.
- Walcott, R. I., Lithospheric flexure, analysis of gravity anomalies and the propagation of seamount chains, in *The Geophysics of the Pacific Ocean Basin and Its Margin*, *Geophys. Monogr. Ser.*, vol. 19, edited by G. H. Sutton, M. H. Manghnani, and R. Moberly, pp. 431-438, AGU, Washington, D. C., 1976.
- Watts, A. B., J. H. Bodine, and C. O. Bowin, Free-air gravity field, Geophysical Atlas of East and Southeast Asian Seas, *Map and Chart Ser. MC-25*, edited by D. E. Hayes, Geol. Soc. of Amer., Boulder, Colo., 1978.